30

Modeling of Surface-bed Reactor for Endothermic and Exothermic Reactions Coupling

Salvatore Vaccaro and Paolo Ciambelli
Department of Chemical and Food Engineering, University of Salerno
Italy

1. Introduction

Hydrogen has acquired great importance in the last decade mainly because its combustion with air does not give rise to pollutant emissions in the atmosphere (either toxic or producing greenhouse effect). Therefore, it is seen as the future transportation fuel at least for urban areas (Jamal & Wyszynski (1994); Moore & Raman, (1998); Kruger, et al., 2003; Lerer et al., 2006). A second reason for the growth of its importance is the proposed use as main energy carrier for fuel cells (Rostrup-Nielsen, 2004). However, hydrogen cannot be considered a fuel in the conventional meaning of the term since it is not available in elemental form in concentrations and amounts suitable for human needs. It is, more appropriately, an energy carrier because it can be produced industrially at reasonable costs from fossil fuels or also from water electrolysis but in a very expensive way (Lincoln, 2006).
The needs for hydrogen of the chemical industry are, generally, satisfied by the process of catalytic steam reforming of fossil fuels, which produces synthesis gas (H_2 and CO) that in turn is used for many important processes including methanol/dimethyl ether (DME) synthesis, ammonia production, olefins oxosynthesis to aldehydes (Marschner et al., 2005), carbonylation, hydrodesulphurization, hyrdrocracking, etc. (Rostrup-Nielsen, 1995) or as feedstock to the Fischer–Tropsch process for liquid hydrocarbons production (Rostrup-Nielsen et al., 2001; Cao et al., 2005).
Commercial processes for methane steam reforming use tubular reactors packed with supported nickel catalysts. In the conventional reactors, strong endothermic reactions occur at high temperatures for high conversion with fast kinetics. In these conditions the reaction becomes diffusion controlled and, therefore, a suitable catalyst structure design play an important role in obtaining high activity and stability. In addition, because of the endothermicity of the steam reforming process, the rate at which heat is transferred from an outside occurring exothermic reaction to the reactor tubes may become controlling.
In recent years, microchannel reactors have been developed for process intensification and used in exothermic and endothermic reactions for their noticeable temperature control and improved mass transfer (Ehrfeld et al., 2000; Jensen, 2001; Schubert et al., 2001; Lerou & Ng (1996); Holladay et al., 2004). The use of microchannels potentially minimizes the temperature gradient and allows the reaction occurring at a higher average temperature so that the process efficiency is enhanced. A structured metallic support, with high thermal

conductivity, can be used as a substrate of catalysts and integrated for plate-type reactors and microchannel reactor applications. Thin layers of catalyst coating (typically of the order of 10-100 nm) on the metal substrate give much shorter transport distances than that of conventional catalysts (Wang et al., 2005). Beside industrial applications, multifunctional autothermal reactor concepts have been proposed for the thermal coupling of endothermic reactions with auxiliary combustion reactions for an efficient heat-integrated process. These concepts aim to minimizing fuel consumption and waste heat production in stand-alone hydrogen production, which gains increasing interest for innovative power generation systems, e.g., fuel cells (Kolios et al., 2004).

Surface-bed reactors or plate-type reactors and microchannel reactors with microstructured catalysts have been suggested for steam reforming of hydrocarbons or for exothermic reactions (Tronconi & Groppi (2000); Zanfir & Gavriilidis (2003); Robbins et al., 2003; Kolios et al., 2004; Cao et al., 2005). In developing such reactors, the knowledge of the temperature profile within the reactor is important for designing and optimizing the catalysts structure and the reactor geometry to achieve the best performance. However, temperature measurement within the catalyst structures in such a small dimension devices becomes difficult, either due to insufficient room for a thermocouple or to potential interference with local fluid-dynamics (Cao et al., 2005). Therefore, to evaluate not only the local temperature profiles but the whole reactor performance in terms of conversion and selectivity, accurate descriptive or predictive models are necessary. As a mature technology, methane steam reforming kinetics in a conventional fixed bed reactor has been well described (Bridger, 1980; Rostrup-Nielsen et al., 1988). Pseudo-homogeneous two-dimensional models have been used to simulate operation of the catalytic steam reformers (Xu & Froment (1989a); Kvamsdal et al., 1999). Numerous studies have focused on the kinetics of methane steam reforming (Akers & Camp (1955); Allen et al., 1975; Aparicio, 1997; Luna and Becerra 1997; Craciun et al., 1998; Xu & Froment, 1989b; Hou & Hughes, (2001)), especially on Ni catalysts.

Nevertheless, few modeling attempts of methane steam reforming in surface-bed or plate-type reactors are currently available in the open literature (Avci et al., 2001; Zanfir & Gavriilidis (2003); Kolios et al., 2004; Cao et al., 2005). They are 2D and all include simplifying assumptions. For instance, Zanfir & Gavriilidis (2003) adopted a two-dimensional geometry for the gas phase and the solid wall, while the catalyst layers were modeled by one-dimensional approach. The motion field was assumed fully developed laminar flow in both endothermic and exothermic channel. In addition, due to its small thickness, the catalyst layer was considered isothermal in the transverse direction and the pressure drop along the channels was neglected.

In this context, the present work aimed at studying an autothermal, dual catalyst, surface-bed reaction system for hydrogen production from methane for portable devices. Such devices were thought to be employed for the remote production of electric power via endothermic reactions, such as ammonia decomposition or hydrocarbon steam reforming (endothermic reactions), to produce hydrogen for fuel cells. Heat for the endothermic reaction is provided by an exothermic reaction occurring over the other face of the plate where the reforming reaction occurs. The reaction system was mathematically modeled in steady-state both 2D and 3D and model solutions by a FEM software (COMSOL Multiphysics) were carried out.

The purpose of the stationary model discussed here is to predict the methane conversion and temperature distribution within the microstructure in a 2D and 3D geometry. A sensitivity study of the simulation was used to allow the design of the catalyst structure and reactor geometry to reduce the mass/heat transfer limitation in the process and take advantage of the fast kinetics of the methane steam reforming reaction.

2. Reacting system

The main chemical reactions occurring in the reactor are:

- Methane steam reforming:

$$CH_4 + H_2O \leftrightarrow CO + 3H_2 \qquad \Delta H_1^0 = 206.1\ kJ/mol \tag{1}$$

For which the reaction rate equation utilized in the calculation is:

$$r_1 - \frac{\frac{k_1}{p_{H_2}^{2.5}} \cdot \left(p_{CH_4} \cdot p_{H_2O} - \frac{p_{H_2}^3 \cdot p_{CO}}{K_{e,1}} \right)}{Den^2} \qquad \left[\frac{kmol}{kg_{cat} \cdot h} \right] \tag{1'}$$

- Water gas-shift:

$$CO + H_2O \leftrightarrow CO_2 + H_2 \qquad \Delta H_2^0 = -41.0\ kJ/mol \tag{2}$$

For which the corresponding rate equation is:

$$r_2 = \frac{\frac{k_2}{p_{H_2}^{3.5}} \cdot \left(p_{CO} \cdot p_{H_2O} - \frac{p_{H_2} \cdot p_{CO_2}}{K_{e,2}} \right)}{Den^2} \qquad \left[\frac{kmol}{kg_{cat} \cdot h} \right] \tag{2'}$$

where

$$Den = 1 + K_{CO} \cdot p_{CO} + K_{H_2} \cdot p_{H_2} + K_{CH_4} \cdot p_{CH_4} + \frac{K_{H_2O} \cdot p_{H_2O}}{p_{H_2}} \tag{2''}$$

The rate equations (1′) and (2′) are those derived by Xu & Froment (1989b), for a catalyst containing 15.2% Ni supported on MgO-αAl_2O_3.

- Methane combustion:

$$CH_4 + 2O_2 \leftrightarrow CO_2 + 2H_2O \qquad \Delta H_3^0 = -803.2\ kJ/mol \tag{3}$$

For which the corresponding rate equation is:

$$r_3 = k_3 \cdot c_{CH_4} \qquad \left[\frac{kmol}{m^3 \cdot s}\right] \tag{3'}$$

The rate equation (3′), suggested in the literature (Zanfir & Gavriilidis (2003)), is valid for a catalyst containing Pt supported on α-Al_2O_3

Pre-exponential factors $k_{k,0}$		Activation energy, E_{ak} (kJ/mol)
$k_{1,0}$ (kmol $bar^{0.5}$/(kg_{cat} ·s))	1.1736×10^{12}	240.1
$k_{2,0}$ (kmol/(kg_{cat}·s·bar))	1.955×10^{6}	67.13
$k_{3,0}$ (s^{-1})	4.0×10^{8}	90.0
Pre-exponential factor $K_{i,0}$		Heat of adsorption, ΔH_i (kJ/mol)
$K_{CO,0}$ (bar^{-1})	8.23×10^{-5}	- 70.65
$K_{CH4,0}$ (bar^{-1})	6.65×10^{-4}	- 38.28
$K_{H2O,0}$ -	1.77×10^{5}	88.68
$K_{H2,0}$ (bar^{-1})	6.12×10^{-9}	- 82.9
Equilibrium constants		
$K_{e,1} = \exp(-26830/T + 30.114)$ (bar^2)		
$K_{e,2} = \exp(4400/T - 4.036)$		

Table 2. Kinetic parameters for the reaction rate equations

Partial pressures of gases p_i in equations (1′), (2′) and (2″) were correlated to their own concentrations by the ideal gas law. The values of pre-exponential factors and activation energies used in the Arrhenius expression for the kinetic constants, i.e. $k_k = k_{k,0} \exp(-E_{ak}/RT)$, in equations (1′), (2′) and (3′) are reported in Table 2 with the relevant dimensions. In the same Table the values of the pre-exponential factors and of the heats of adsorption, taken from the literature (Perry & Green, 1997) and used in Van't Hoff expression, i.e. $K_i = K_{i,0} \exp(-\Delta H_i/RT)$, for the constants in equation (2″) and the expressions of the equilibrium constants $K_{e,1}$ and $K_{e,2}$ in equations (1′) and (2′) are also shown.

3. Reactor model

3.1 Physical description

A 2D scheme of the reactor model is shown in Figure 1 where the various parts are identified by numbers. The system is symmetric with respect to the channel 5 centerline and then the parts 1 and 9, 2 and 8, 3 and 7 and 4 and 6 are identical pairs. With reference to Figure 1, reforming gas goes through the central channel 5 while combustion gas through channels 1 and 9. Parts 3 and 7 represent metallic plates where the structured catalysts layers for combustion (2 and 8) and steam reforming (4 and 6), respectively, lie. It is not very different from modular reactors made of stackable plates suggested in the literature (Xu & Froment (1989a); Loffler et al., 2002). The main difference is that in this case the external boundaries 10 and 11 (in Figure 1) are surfaces with no slip gas velocity while in the recalled case they were symmetry surfaces.

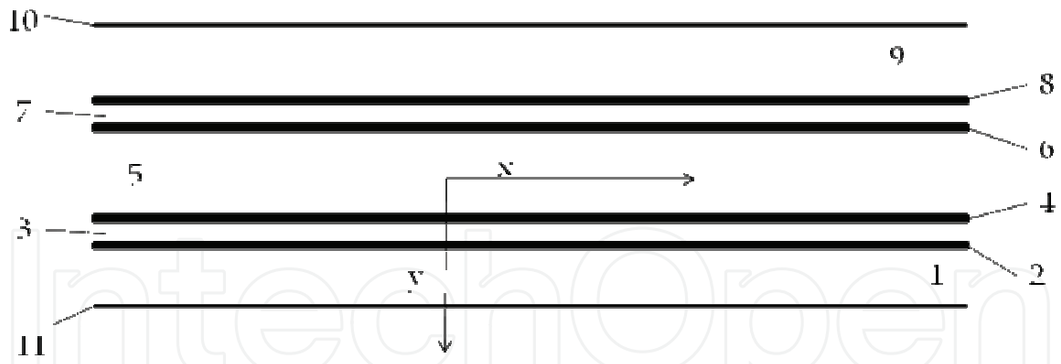

Figure 1. Reactor scheme

With respect to conventional catalytic reactors, where a bed of catalytic solid particles fills the reactor volume and the gas crosses the bed, in the present case the catalytic solid particles are located on the lateral surfaces of the reactor thus forming a surface bed. Actually, in the case in the object the true reactor is the catalyst layers while the homogeneous portions of the reactor (channels) act merely as ducts.

3.2 Model

A three-dimensional heterogeneous steady-state model was developed in order to describe velocity, concentration and temperature distributions inside the surface-bed reactor system with structured catalysts. The model consists of the material, energy and momentum balances equations and contains the constitutive equations for physical chemistry properties of the reactants species and the kinetic expressions for the reactions as found from the literature and presented above.

The model assumes that: a) the variations of density due to the change of gas composition and temperature are small so that incompressible Navier-Stokes motion equation applies; b) on the combustion side only the methane total oxidation reaction to H_2O and CO_2 occurs; c) on the reforming side only the methane steam reforming and the water gas shift reactions occur; d) reactions occur only inside the catalyst layers where, instead, convective momentum is not present; e) conductive heat transfer is the only transport phenomenon occurring inside the metallic plates; f) as suggested in the literature (Hou & Hughes (2001); Zanfir. & Gavriilidis (2003)), carbon formation and deposition due to side reactions can be neglected by using an excess of steam, that is a minimum steam/methane molar ratio of 1.7; f) body forces are neglected, the reacting species being gaseous.

The velocity variation in the reactor takes into account the influence of temperature and composition changes so that the global mass balance is satisfied:

$$\iint_0^{ts} \rho_i u_x \, dy \, dz \,\big|_{x=0} = \iint_0^{ts} \rho_i u_x \, dy \, dz \,\big|_{x=x} \tag{4}$$

Reactor performance were evaluated by the methane conversions, calculated by integrating the local molar flow rates:

$$X_{CH4}(x) = 1 - \frac{\iint_0^{ts} C_{CH4} \cdot u_x \, dy \, dz \,\big|_{x=x}}{\iint_0^{ts} C_{CH4} \cdot u_x \, dy \, dz \,\big|_{x=0}} \tag{5}$$

According to Figure 1, for each catalyst layer and channel and for the metal sheets the due momentum, energy and mass balances were set together with the proper boundary conditions in the rectangular coordinates (x–y–z) (Cartesian coordinates are indicated in Figure 1 and the z direction is perpendicular with respect to the scheme) with dependent variables: velocity components, pressure, temperature (T) and species concentrations (c_i). Equations vectorial formulation are reported in the following so they are valid for both 2D and 3D formulations.

Combustion channels 1 and 9 and steam reforming channel 5

Momentum balance

$$\rho\,\vec{v}\cdot\nabla\vec{v} = \nabla\left(-P\vec{I} + \mu\cdot\left(\nabla\vec{v} + \nabla(\vec{v})^T\right)\right) \tag{6}$$

$$\nabla\cdot\vec{v} = 0 \tag{7}$$

Boundary conditions are:

- specified velocity with normal component at the channel ingress $\vec{v}\cdot\vec{n} = v_0$
- no slip at the channel boundaries in the y (2D and 3D) and z (3D) directions $\vec{v} = 0$
- specified pressure at the channel exit $P = P_0$

With reference to Figure 1 for the momentum balance equations the boundaries of channels 1 and 9 are the external boundaries (10 and 11) of the reactor and the internal boundaries between the channels and the catalyst layers, respectively, while the boundaries of channel 5 are the internal boundaries between the channel and the catalyst layers.

Energy balance

$$\nabla\cdot(-k\nabla T) = \rho c_p\vec{v}\cdot\nabla T \tag{8}$$

Boundary conditions are:

- specified temperature at the channel ingress $T = T_0$
- convective heat flux at the channel exit $\vec{n}\cdot\nabla(-kT) = 0$
- *Channels 1 and 9* : no heat flux through the channel external boundaries in the y (2D and 3D) and z (3D) directions, i.e. $\vec{n}\cdot(-k\nabla T + \rho c_p T\vec{v}) = 0$ and thermal continuity $\vec{n}\cdot(q_1 - q_2)) = 0 \quad q_l = k_l\nabla T_l + \rho c_{p,l} T_l\vec{v}_l$ at the internal boundaries (*l*: gas phase and catalyst phase).
- *Channel 5:* thermal continuity $\vec{n}\cdot(q_1 - q_2)) = 0\ q_l = k_l\nabla T_l + \rho c_{p,l} T_l\vec{v}_l$ at the internal boundaries (*l*: gas phase and catalyst phase).

Mass balances

$$\nabla\cdot\left(-D_{i,j}\nabla c_i + c_i\vec{v}\right) = 0 \tag{9}$$

Boundary conditions are:

- specified concentrations at the channel ingress $c_i = c_{i,0}$
- continuity through the boundary between the gas phase and the catalyst layer, i.e. $\vec{n}\cdot(N_{i,1} - N_{i,2})) = 0$ where $N_{i,1} = D_{i,j,1}\nabla c_{i,1} + c_{i,1}\vec{v}$ and $N_{i,2} = (-D_{eff,i,j,2}\nabla c_{i,2})$
- convective mass flux at the channel exit $\vec{n}\cdot\left(-D_{i,j}\nabla c_i\right) = 0$

where i and j subscript refers to the i*th* and j*th* specie, respectively.

Catalyst Layers 2 and 8

Energy balance

$$\nabla \cdot (-k_{cat}^{co} \nabla T) - r_3 \Delta H_3 \tag{10}$$

Boundary conditions are:

- thermal continuity at the layers boundaries in the y directions (2D and 3D) $\vec{n} \cdot (q_1 - q_2)) = 0$ $q_l = k_l \nabla T_l + \rho c_{p,l} T_l \vec{v}_l$ (*l*: gas phase and catalyst phase).
- thermal insulation at the layer boundaries in the x (2D and 3D) and z (3D) directions $\vec{n} \cdot (-k \nabla T + \rho c_p T \vec{v}) = 0$

Mass balances

$$\nabla \cdot (-D_{eff,i,j} \nabla c_i) = \theta_i r_3 \tag{11}$$

being θ_i the stoichiometric coefficient of the i*th* specie.

Boundary conditions are:

- continuity through the boundary between the layer and the gas phase $\vec{n} \cdot (N_{i,1} - N_{i,2})) = 0$ where $N_{i,1} = D_{i,i,1} \nabla c_{i,1} + c_{i,1} \vec{v}$ and $N_{i,2} = (-D_{eff,i,j,2} \nabla c_{i,2}) = 0$ and no mass flow $\vec{n} \cdot (-D_{eff,i,j} \nabla c_i + c_i \vec{v}) = 0$ between the layer and the metal sheets in the y (2D and 3D) direction
- no mass flux through the layer boundaries in the x (2D and 3D) and z (3D) directions $\vec{n} \cdot (-D_{eff,i,j} \nabla c_i + c_i \vec{v}) = 0$

Metal sheets 3 and 7

Energy balance

$$\nabla \cdot (-k_s \nabla T) - 0 \tag{12}$$

Boundary conditions are:

- thermal insulation at the sheet boundaries in the x (2D and 3D) and z (3D) directions $\vec{n} \cdot (-k_s \nabla T) = 0$
- thermal continuity on the sheet boundaries in the y direction (2D and 3D) $\vec{n} \cdot (q_1 - q_2)) = 0$ $q_i = k_i \nabla T_i$

Catalyst Layers 4 and 6

Energy balance

$$\nabla \cdot (-k_{cat}^{sr} \nabla T) = r_1 \Delta H_1 + r_2 \Delta H_2 \tag{13}$$

Boundary conditions are:

- thermal insulation at the layer boundaries in the x (2D and 3D) and z (3D) directions $\vec{n} \cdot (-k_{cat}^{sr} \nabla T) - 0$
- thermal continuity on the layers boundaries in the y direction (2D and 3D) $\vec{n} \cdot (q_1 - q_2)) = 0$ $q_i = k_i \nabla T_i$

Mass balances

$$\nabla \cdot (-D_{eff,i,j} \nabla c_i) = \theta_{1,i} r_1 + \theta_{2,i} r_2 \tag{14}$$

being $\theta_{j,i}$ the stoichiometric coefficients of the i specie in the j reaction.

Boundary conditions are:

- continuity through the boundary between the layer and the gas phase $\vec{n} \cdot (N_{i,1} - N_{i,2})) = 0$ where $N_{i,1} = D_{i,j,1} \nabla c_{i,1} + c_{i,1} \vec{v}$ and $N_{i,2} - (-D_{eff,i,j,2} \nabla c_{i,2}) - 0$ and no mass flow $\vec{n} \cdot \left(-D_{eff,i,j} \nabla c_i + c_i \vec{v}\right) = 0$ between the catalyst layer and the metal sheet in the y (2D and 3D) direction
- no mass flux through the layer boundaries in the x (2D and 3D) and z (3D) directions $\vec{n} \cdot (-D_{eff,i,j} \nabla c_i + c_i \vec{v}) = 0$

In the balances above the gas densities were calculated using the ideal gas law whereas for catalyst density a constant value was assumed. Viscosities and thermal conductivities of the gaseous species refer to the values of the component largely in excess in the specific gas mixtures, that is H_2O for the steam reforming channel and air for the combustion channels. Their dependence of the temperature was excerpted from experimental values from the literature (Perry & Green (1997)) and included as interpolated functions inside the calculation software. To work out heat capacities, expressions such as:

$$c_p = A + BT + CT^2 \tag{15}$$

were used where A, B and C were evaluated by the regression of an expression (Perry & Green (1997) such as:

$$c_{p,i} = C1 + C2\left[\frac{\frac{C3}{T}}{\sinh\frac{C3}{T}}\right]^2 + C4\left[\frac{\frac{C5}{T}}{\cosh\frac{C5}{T}}\right]^2 \tag{16}$$

The diffusivity coefficients were calculated for a binary mixture between component *i*th and H_2O (in the reforming channel) or air (in the combustion channels). The effective diffusion coefficient inside the catalyst layer is (Perry & Green (1997):

$$D_{eff,i,j} = \frac{\varepsilon}{\tau}\left[\frac{1}{D_{i,j}^k} + \frac{1}{D_{i,j}}\right]^{-1} \tag{17}$$

where ε is the catalyst porosity, τ the tortuosity, $D_{i,j}^k$ and $D_{i,j}$ the Knudsen diffusion coefficient and the molecular diffusion coefficient of the i*th* specie in the j*th* specie, respectively. Molecular diffusion coefficients were evaluated using (Perry & Green (1997)):

$$D_{i,j} = \frac{0.1013\, T^{1.75}\left(\frac{1}{M_i} + \frac{1}{M_j}\right)^{0.5}}{\pi\left[\left(\sum \varphi_i\right)^{1/3} + \left(\sum \varphi_j\right)^{1/3}\right]^2} \tag{18}$$

where T is the temperature in [K], π the total pressure of the system in [Pa], M_i and M_j the molecular weights of i*th* and j*th* species, respectively, and φ_i the atomic diffusion volumes, characteristic for each component (Perry & Green (1997)). Knudsen diffusion coefficients were evaluated using (Perry & Green (1997)):

$$D_{i,j}^k = 97\, R_p \sqrt{\frac{T}{M_{i,j}}} \tag{19}$$

where R_p is the mean pore radius and T the temperature into the catalyst.

3.3 Numerical stuff and reference case simulation

The finite element solution algorithm was completed using COMSOL Multiphysics (Comsol, Inc., version 3.3a). Multiphysics modules of incompressible Navier-Stokes, convection–diffusion and conduction–convection were applied, when appropriate, to the three-phase domains. Meshing parameters were different for the 2D and the 3D FEM schemes. In particular, in the case of 2D a mapped mesh scheme was employed with rectangular extra fine meshes and edge vertex distribution as follows: longitudinal edges 100:1; transverse edges 5:1 (metallic plate) and 10:1 (catalyst layers and channels). In the case of 3D predefined mesh sizes, extra coarse with characteristics listed in Table 3, were employed.

Number of degrees of freedom	381162
Number of mesh points	6976
Number of elements	33702
Tetrahedral	33702
Number of boundary elements	12840
Triangular	12840
Number of edge elements	740
Number of vertex elements	24
Minimum element quality	0.158
Element volume ratio	0.015

Table 3. Mesh Statistics

A reference case with given reactor geometric configuration and operating conditions was chosen to carry out a reference case simulation. Other simulations were carried out to explore the influence on the reactor performance of specific geometrical and/or operating parameter changes. The conditions used in the calculations for the reference case are listed in Table 4. Inlet conditions for the reforming side are similar to those used by Xu and Froment (1989b), but for the total pressure close to atmospheric in our case, 29 bar, characteristic of industrial operation, in the kinetics from Xu & Froment. This because, as suggested in the literature (Kolios et al., 2004), small-scale hydrogen production, which is the potential application for such type of reactor is expected to operate at low pressure.
This represents a limit of the present work. However, similar detailed rate equations for the investigated reacting system are not available at ambient pressure in the literature. Data reported in Table 4 show that the inlet reforming reaction mixture has a steam/methane ratio of 3 and contains trace amounts of CO_2, H_2 and CO. On the methane combustion side, the air–methane mixture has a 40% air excess with respect to stoichiometric. The inlet temperature of both streams is 800 K that is close to that typical of industrial steam reforming. The inlet methane mass flow rate in the reforming channel is fixed at 1.67 cm^3/s at STP, while the inlet methane mass flow rate in the combustion channel is obtained from an overall heat balance. The data for reforming catalyst used in the calculations are typical for such a reaction and similar to that used by Xu & Froment (1989a) for a catalyst containing 15.2% Ni supported on MgO-αAl_2O_3.

Gas phase	Reforming channel	Combustion channels
Inlet conditions		
co-current flow		
compositions, vol. %		
H_2O	66.66	
CH_4:	33.33	7.50
CO_2	$1\ 10^{-3}$	
CO	$1\ 10^{-3}$	
O_2		19.43
N_2		73.07
H_2	$1\ 10^{-3}$	
temperature	800 K	800 K
CH_4 mass flow rate, cm^3/s (STP)	1.67	0.417
pressure	101 kPa (channel outlet)	101 kPa (channel outlet)
channel width, m	$2\ 10^{-3}$	$1\ 10^{-3}$
channel height, m	$1.0\ 10^{-2}$	
average velocity, m/s	0.97	0.87
channel length, m	$5\ 10^{-2}$	
Catalyst layers		
thickness (δ_c), µm	200	
Average pore radius, nm	15	
porosity	0.5	
tortuosity	4	
Metal plates		
Thickness, m	5 10-4	
material	aluchrom	
Thermal conductivity, w/(m K)	Temperature dependent	

Table 4. Data used for reference case calculations

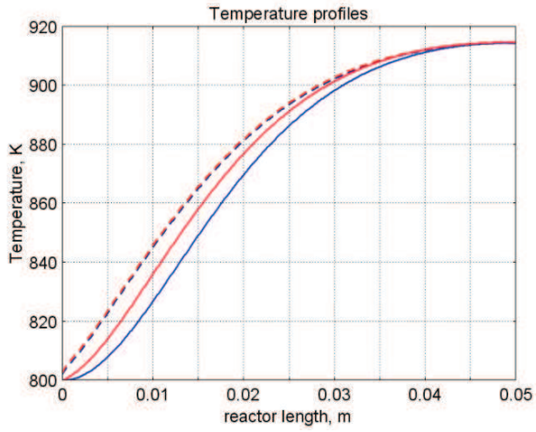

Figure 2. Temperature space profiles along the reactor: centerline of the reforming channel (solid blue), centerline of the combustion channel (solid red), centerline of the reforming catalyst (dashed blue) and centerline of the combustion catalyst (dashed red)

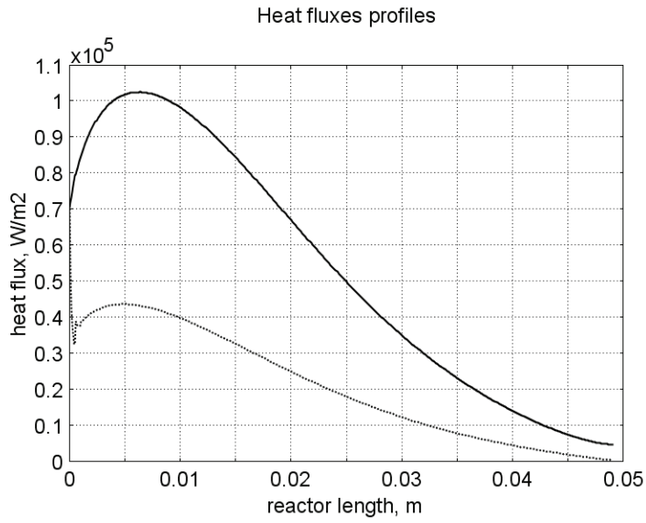

Figure 3. Axial profiles of heat flux in the y direction adjacent to the reforming catalyst: in the metallic plate (solid line), in the reforming channel (dotted line)

The catalyst layer density is assumed to be 2300 kg/m^3. For both type of catalyst layers an average pore radius of 15 nm, together with a porosity of 0.5 and a tortuosity factor of 4 are considered. These values are typical for both combustion and reforming catalysts (De Deken et al., 1982; Xu & Froment, 1989 b; Groppi et al., 1995).

4. Results

4.1 Thermal behaviour

Given the symmetry of the reactor, for both 3D and 2D simulations only half of the reactor was simulated by substituting the proper boundary conditions (symmetry) in place of the lacking half. Results in simulations performed with the 2D model, under the reference case conditions, are shown in Figures 2-7. The first aspect to consider is the thermal coupling of steam reforming with catalytic combustion in terms of evolution of both exothermic and endothermic conversion. Figure 2 shows the temperature longitudinal profiles on the centerlines of the combustion and the reforming channels, and in the combustion and reforming catalysts. The profiles are very close each other and they increase from the inlet value of 800 to 914 K at the reactor outlet. Therefore, the catalytic combustion provides the necessary heat flux to heat up both reaction mixtures and to simultaneously drive the endothermic process. A methane conversion at the reactor outlet of 0.89 for combustion and 0.74 for reforming are achieved. Figure 3 shows the axial profiles of the absolute values of the heat fluxes in the y direction at the boundaries of the reforming catalyst. One profile (solid line) is the heat flux from the metallic plate towards the reforming catalyst, the other the heat flux from the reforming catalyst to the gas mixture in the reforming channel. The two profiles present similar shapes with a maximum at 7 mm and 5 mm from the reactor entrance (distances within which the profiles are increasing). The difference between the profiles represents the heat absorbed by the reforming reaction system (eq.s (1) and (2)). The maxima heat fluxes generated and consumed reach values of the order of 10^5 W/m^2 i.e. 10 W/cm^2 that, considering the very small temperature gradients (Figure 2), is a very high value with respect to that attainable in industrial practice.

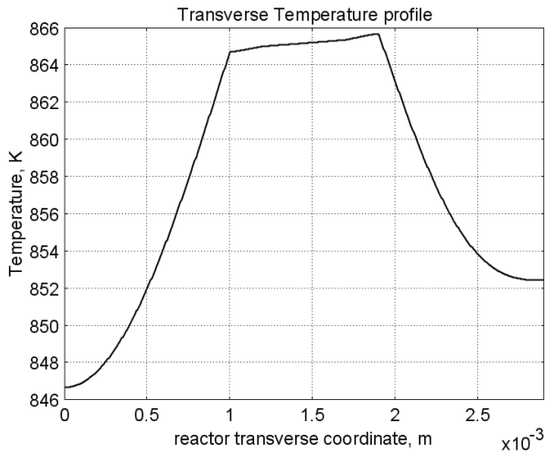

a)

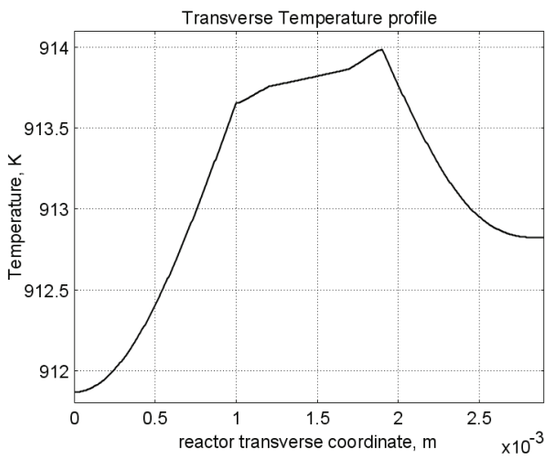

b)

Figure 4. Reactor temperature transverse profiles: a at 1.5 cm from the reactor entrance; b at 1.0 cm from the reactor outlet. From 0 to 1: reforming channel. From 1 to 1.2: reforming catalyst. From 1.2 to 1.7: metallic plate. From 1.7 to 1.9: combustion catalyst. From 1.9 to 2.4: combustion channel

A further aspect to be examined is the magnitude of the transverse temperature gradients. From Figure 2 it is already evident that the four profiles are very close each other. However, the transverse temperature gradients can be better analyzed from Figure 4 where the transverse temperature profiles at 1.5 cm (Figure 4a) from the reactor entrance and at 0.5 cm (Figure 4b) from the reactor outlet are shown. In particular, Figure 4a, which pertains to the distance from the reactor inlet where the highest transverse temperature gradients develop, evidences that the maximum temperature difference between reforming and combustion catalyst is 0.7 K while the maximum difference between the reforming and combustion channels is less than 10 K although that inside the reforming channel is almost 20 K. Much lower differences can be observed close to the reactor outlet. Specifically, Figure 4b shows that the maximum temperature difference between reforming and combustion catalyst is 0.1 K, that between the reforming and combustion channels is less than 1 K and that inside the reforming channel is almost 2 K. As a result, the high thermal conductivity of the metallic

wall makes possible an efficient heat transfer at a temperature difference of the order of tenths of K. With reference to Figure 4, it must be remarked that the value 0 of the transverse coordinate represents the centre of the reactor and the centre of the reforming channel. Therefore, at that point there is not a physical boundary, the heat flux and the momentum flux are both zero and the x component of the gas velocity is maximum. On the contrary, the value 2.9 10^{-3} m of the transverse coordinate represents a solid wall that is the external boundary of the reactor and the boundary of the combustion channel. This means that the heat flux is zero, both components of the gas velocity are zero and the momentum flux is not zero. This is one of the reasons because for the same distance in the transverse direction (y) the gas phase temperature difference in the reforming channel results always larger than that in the combustion channel (Figures 2, 4a and 4b).

4.2 Mass transfer and chemical reactions

The concentration on the centerline of the reforming channel of the various species involved in the reactions occurring within the reforming catalyst are shown in Figure 5. This yields an overall picture of the reactor performance. The hydrogen concentration steadily increases from the initial value to about 9 mol/m^3 resulting the most abundant component in the exit gas mixture The ratio between the hydrogen concentration and CO concentration is very high (about 9).

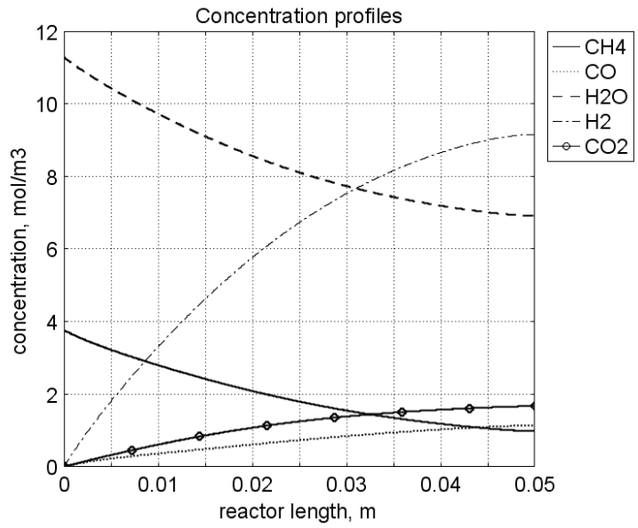

Figure 5. Axial profiles of species concentrations on the centerline of the reforming channel

One important aspect to determine is the effect of interphase mass transport resistance. Figure 6a shows the methane concentration axial profiles on the centerlines of the combustion channels and of the combustion catalyst while Figure 6b shows the correspondent profiles for the reforming section of the reactor. From these Figures the differences between the channel and the catalyst profiles in each section yield a measure of the resistance to the interphase transport. As expected, in the combustion section the axial methane concentration profiles both in the channel and in the catalyst show an exponentially decreasing trend, which reflects the relatively simple kinetics of the reaction. In contrast, a more complex trend is shown by the axial methane concentration profile in the catalyst because of the non linearity of the kinetics and the simultaneous occurrence of two

reactions (eq.s (1) and (2)). Another aspect to examine is the size of the concentration gradients in the transverse direction. These can be appreciated from Figure 7 where the transverse methane concentration profiles at 1.5 cm from the reactor inlet and at 0.5 cm from the reactor outlet are shown. In particular, the first profile, which pertains to the distance from the reactor inlet where the highest transverse temperature gradients develops, evidences that the gradients inside the reforming and the combustion channels are negligible with respect to the gradients in the catalyst phase. The order of magnitude of these latter range from 10^5 mol/m^4 close to the reactor inlet to 10^4 mol/m^4 in the remaining part of the reforming catalyst and in all the combustion catalyst too.

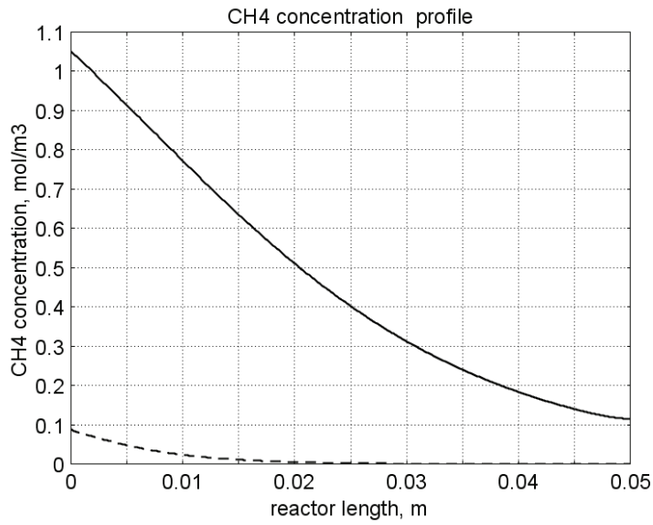

a)

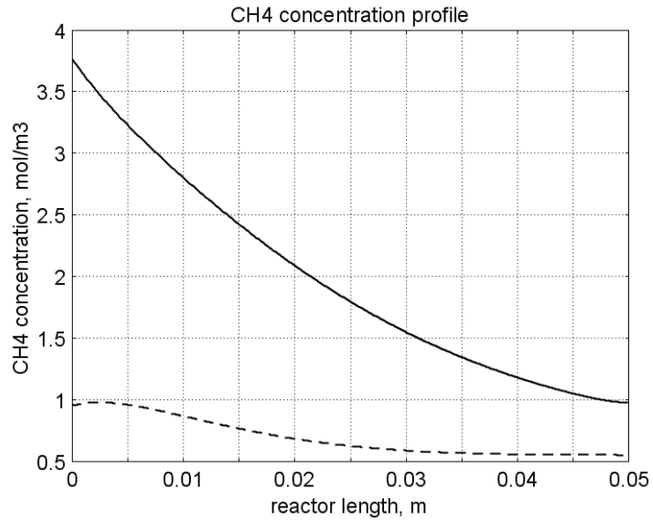

b)

Figure 6. Axial methane concentration profiles along the reactor: (a) solid line combustion channel, dashed line combustion catalyst; (b) solid line reforming channel, dashed line reforming catalyst

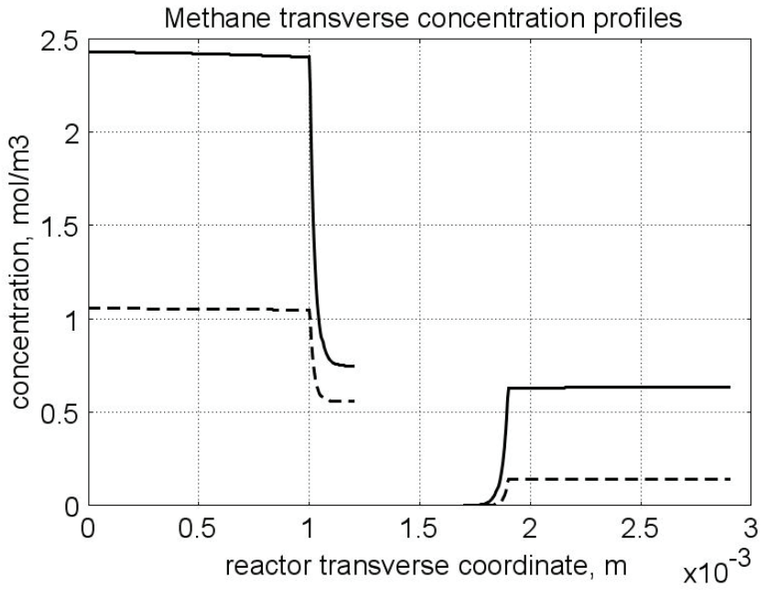

Figure 7. Methane concentration transverse profiles at 1.5 cm from the reactor entrance (solid line) and at 1.0 cm from the reactor outlet (dashed line). From 0 to 1: reforming channel. From 1 to 1.2: reforming catalyst. From 1.2 to 1.7: metallic plate. From 1.7 to 1.9: combustion catalyst. From 1.9 to 2.4: combustion channel

4.3 Methane concentration in the combustion channel

A basic requirement of the system in the object, which is thought to be used for energy feeding of portable electric devices, should be the complete reliability with respect to possible uncontrolled rises in temperature or even to a possible explosion hazard. In this view, the coordination between exothermic and endothermic reaction rates appears fundamental. However, even in the case such a coordination occurs, the possible progress of the combustion reaction in the homogeneous phase may represent an hazard. In addition, if the concentration of the reacting mixture entering the combustion channel is within the flammability limits and the temperature becomes high enough, it could ignite before the reactor inlet. Therefore, for safety purposes the occurrence of the exothermic reaction, here represented by the methane combustion, in the homogeneous phase should be avoided. A possible way to make the system of hydrogen generation intrinsically safe is to feed the combustion mixture at a methane concentration below the LEL (lower explosivity limit). Considering that at STP the LEL of methane in air is about 5 vol%, that the autoignition temperature for air/methane mixtures is around 900 K, the extimated LEL of methane in air at such a temperature should be about 3 vol% (Crowl & Louvar (2002)). Therefore, a safe operating concentration should be about 3 vol%. To this purpose in this work, beside those carried out under the conditions considered in the reference case, other simulations were effected for which, for a given methane mass flow rate, its concentration at the combustion channel inlet was kept below 3 vol%. In this way, the system is intrinsically safe, because the reacting mixture cannot ignite spontaneously. In addition, the simulation becomes more realistic the contribution to the methane combustion of the homogeneous phase being really absent, as implicitly hypothesized in this work.

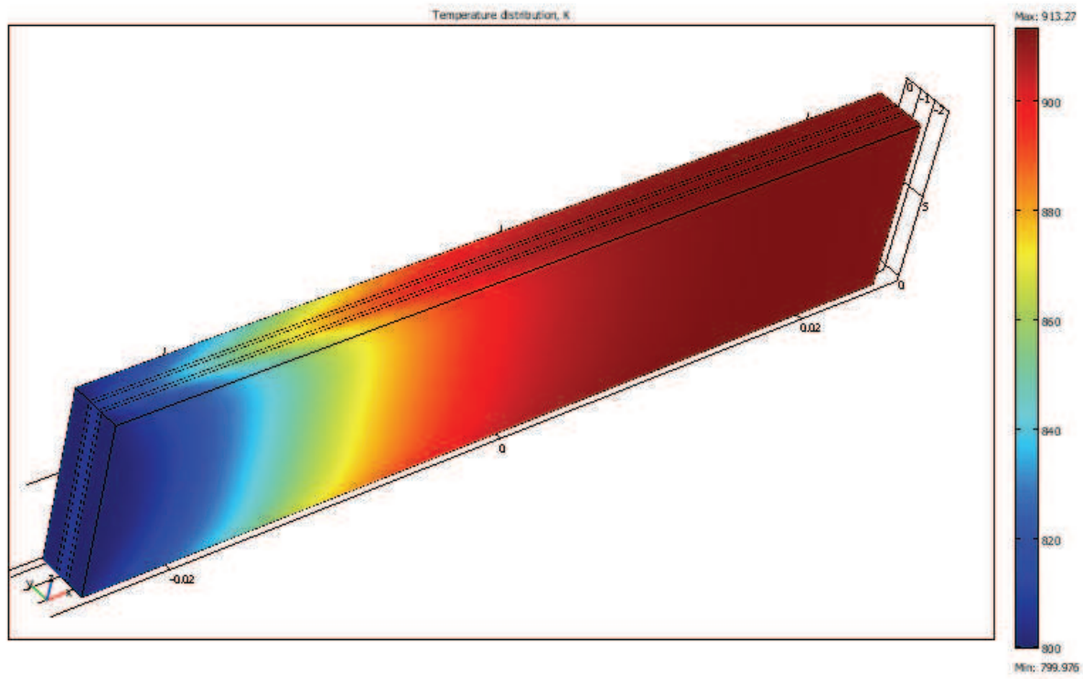

Figure 8. Temperature distribution over the boundaries of the 3D reactor

The comparison of results of runs performed under these conditions with those effected under the conditions of the reference case are reported in the following when analyzing the influence of various parameters on the reactor performance. These simulations are labeled in the paper as **n-expl**. in contrast to the others that are recalled as **expl.**

4.4 Comparison between 2D and 3D results

For given operating conditions some simulations were carried out in both 2D and 3D geometry. In principle, a plane 2D geometry represents a slice of the reactor where the z dimension is greatly prevalent with respect to the y dimension. Actually, the model reactor has not such characteristics, the length in the z dimension being 10 mm, that is only 5 times the reforming channel width. This means that the boundary effects due to the presence of the boundary walls in the z direction may have a significant influence on the velocity, temperature and species concentration profiles that certainly influence the overall reactor performance. Figures 8 shows the temperature distribution over the boundaries of the 3D reactor obtained under operating conditions of the reference case. From this Figure the effect of the boundaries along the z direction appears evident.

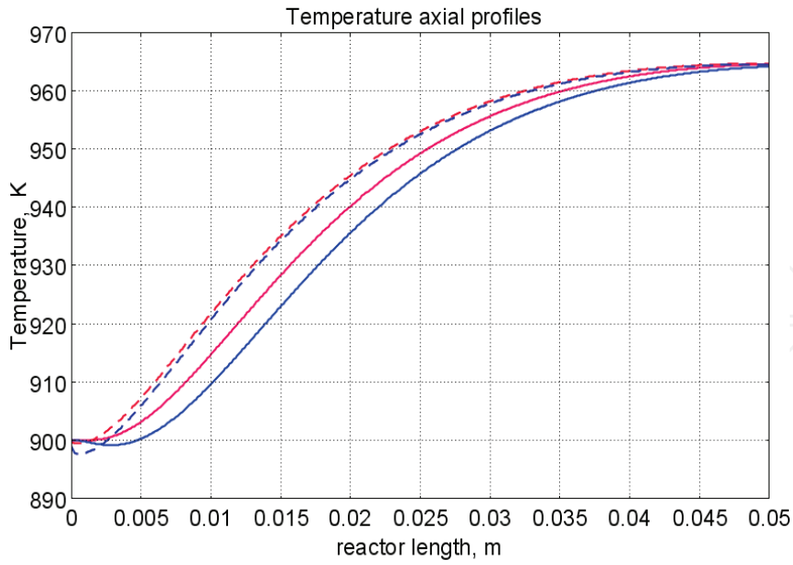

Figure 9. Temperature space profiles along the reactor calculated with the 2D model. (for the legend see caption to Figure 2)

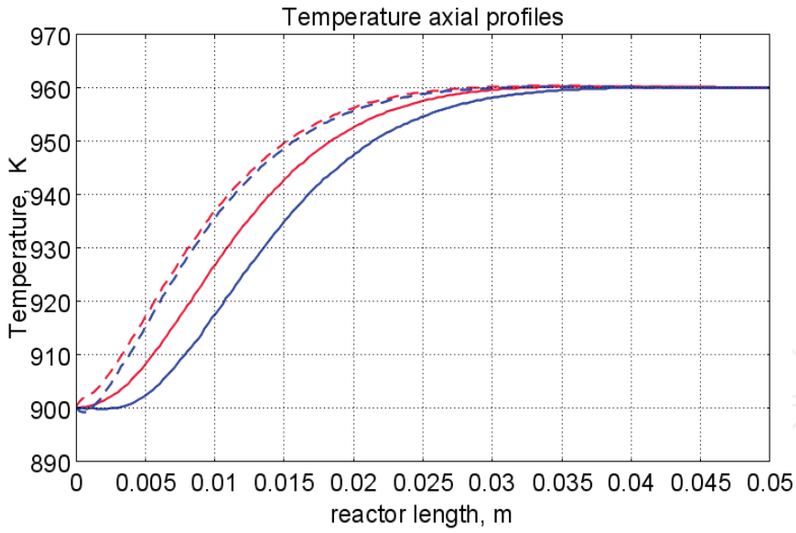

Figure 10. Temperature space profiles along the reactor calculated with the 3D model. (for the legend see caption to Figure 2)

Figures 9 and 10 show the reactor temperature longitudinal profiles on the centerlines of the combustion and the reforming channels, and on the centerline of the combustion and reforming catalysts in the case of 2D and 3D geometry models, respectively. Both were calculated under the same operating conditions, i.e.: same inlet mass flow rates and compositions of the reference case (expl.) but inlet temperature of 900 K. In the case of the

3D simulation (Figure 10) the temperature profiles are those lying over a xy plane intersecting the reactor in the middle of its height along z. The two sets of profiles appear quite similar: the temperatures in the combustion section (catalyst and channel) are always slightly higher than the corresponding ones in the reforming section. However, a closer inspection reveals some significant differences. In the 2D case the temperature, after an initial slow growth, increases steadily from 900 K at the reactor inlet up to 965 K at the reactor outlet while in the other case it grows faster, reaches 960 K at 60% of the reactor length and remains constant up to the outlet. Another difference is represented by the larger transverse temperature gradients of the 3D case with respect to 2D. In the 2D case they are comparable with those observed in Figure 2 for the reference case while in the 3D case they are almost double. This is true for all combinations, i.e. catalyst-catalyst, catalyst-channel and channel-channel. On the whole, the 3D case shows a faster progress of the reactions with consequent need for faster heat transfer. These differences in the thermal behaviour between 2D and 3D simulations persist when the comparison is extended to other operating conditions and, in addition, they reflect the better overall performance of the 3D reactor with respect to the 2D, as can be seen by the following discussion.

The quantitative comparison between the 2D and 3D simulations was made with respect to the main results, i.e. the methane conversion in both the combustion and the steam reforming channels, as obtained from equation 5. Further, beside the methane conversions, other parameters are employed, i.e. a) the gas hourly space velocities GHSV in the combustion and steam reforming sides of the reactor, calculated as ratio between gas flow rates at the reactor inlet temperature and volume of catalyst; b) the maximum temperature reached in the reactor; c) the mean gas residence time, t_{rm}, in both the combustion and the reforming channel, calculated as ratio between the gas flow rates at the reactor inlet temperature and the volume of the channel; and d) the hydrogen yield , φ_{H2}, evaluated as ratio between the amounts of methane reacted and hydrogen produced. GHSV and t_{rm} were useful to allow the comparison of simulations carried out by changing the catalyst volume or the channel width, as discussed later. Results of simulations carried out with the 2D and 3D models under various operating conditions are reported in Table 5. Those referring to the operating conditions of the reference case are listed in the first two rows of such a Table. The other operating conditions are: i) same inlet temperature of the reference case but different methane concentration in the combustion channel (3rd and 4th rows of Table 5) and ii) different inlet temperatures for the two conditions above (5th-8th rows of Table 5). Focusing the comparison on the results of the simulations in 2D and 3D with the same operating conditions, it appears that, in general, the methane conversions at the reactor outlet calculated with the 2D geometry in both the combustion and reforming channels are lower than the correspondent in 3D geometry but in one case ($\mathbf{X_{ch4\text{-}sr}}$ 3rd and 4th rows of the Table**).** This finding reflects the differences in the thermal behaviour discussed above. In any case, such conversions differ by less than 10% but in the last two rows of the Table where the differences are larger. It is worth noting, however, that even in this case the values of the conversions are congruent with the overall results of the simulation. For instance, the lower value of $\mathbf{X_{ch4\text{-}co}}$ in the 2D with respect to the correspondent in 3D results in a lower value of $\mathbf{X_{ch4\text{-}sr}}$ and in a lower maximum temperature reached in the reactor.

Geometry		T_{in}, K	$X_{ch4\text{-}co}$	$X_{ch4\text{-}sr}$	T_{max}, K	$T_{rm\text{-}co}$, ms	$T_{rm\text{-}sr}$, ms	$GHSV_{co}$, h^{-1}	$GHSV_{sr}$, h^{-1}	φ_{H2}
2D	**expl**	800	0.89	0.74	914	0.057	0.026	314840	702884	3.29
3D	**expl**	800	0.96	0.77	914	0.057	0.026	314840	702884	3.33
2D	**n-expl**	800	0.36	0.45	827	0.020	0.026	900588	702884	3.44
3D	**n-expl**	800	0.40	0.41	828	0.020	0.026	900588	702884	3.56
2D	**expl**	900	0.95	0.90	965	0.051	0.023	354194	790745	3.05
3D	**expl**	900	0.99	0.93	960	0.051	0.023	354194	790745	3.00
2D	**n-expl**	900	0.49	0.69	900	0.018	0.023	1013162	790745	3.22
3D	**n-expl**	900	0.68	0.79	920	0.018	0.023	1013162	790745	3.18

Table 5. Comparison of 2D and 3D results obtained under the same operating conditions

For what concerns the hydrogen yield, focusing again the comparison on the results of the simulations in 2D and 3D at the same operating conditions, data show that $\varphi_{H2's}$ obtained with the 2D geometry model are lower than that in 3D model but in one case (7th and 8th row of Table 5**).** It is worth noting that φ_{H2}=3 would be the stoichiometric value if reaction (1) were the only occurring in the reforming catalyst so that the amount exceeding 3 is due to the contribution of reaction (2).

Data in Table 5 also shows the influence on the reactor performance of temperature and inlet methane concentration in the combustion channel. In the case of inlet temperature of 900 K and methane concentration within the explosivity limits (case referring to results in Figures 9 and 10) the methane conversion is practically 1 (3D model) for the combustion reaction and very high for the reforming reactions. However, under these conditions the hydrogen yield is the lowest. In contrast, when the highest hydrogen yield is reached the lowest methane conversion is achieved. Similar considerations can be done for the other results in the Table so that a general trend can be drawn from such results. The higher the maximum temperature reached in the reactor the higher the methane conversions and the lower the hydrogen yield.

4.5 Influence of the channels width

The reactor thermal behaviour and performance was studied for different channels width, W_c, at constant inlet flow rates of the reaction mixtures. Runs were also carried out by keeping constant the mean inlet velocities of reaction mixtures. The variation range for the combustion channels width, $W_{c\text{-}co}$, was 1-1,5 mm and for the reforming channel width, $W_{c\text{-}sr}$, 2-3 mm. All other parameters were kept at their reference case values. Keeping constant the inlet mass flow rates and altering the channel width results in modifying the inlet velocities in the reactor and consequently the mean residence time (t_{rm}) of the gases in the channels but the GHSV's do not change. The results in terms of methane conversions in the combustion and reforming channels are reported in Table 6 for the reference cases (3rd and 4th row in Table) and for cases where the methane concentration in the combustion channels were below the LEL (1st and 2nd row). At constant mass flow rates the influence of the channel width or, better, of t_{rm}, appears negligible under n-expl. conditions with a slight

prevalence of the reactor with narrower channels, and weak under expl. conditions with, in contrast, better performance for the reactor with wider channels. Therefore, it is not possible to draw conclusions.

$W_{c\text{-}sr}$, mm		T_{in}, K	$X_{ch4\text{-}co}$	$X_{ch4\text{-}sr}$	T_{max}, K	$t_{rm\text{-}co}$, ms	$t_{rm\text{-}sr}$, ms	$GHSV_{co}$, h^{-1}	GHSVsr, h^{-1}
2	n-expl	800	0.36	0.45	827	0.020	0.026	900588	702884
3	n-expl	800	0.34	0.44	819	0.030	0.038	900588	702884
2	expl	800	0.89	0.74	914	0.057	0.026	314840	702884
3	expl	800	0.92	0.81	940	0.086	0.038	314840	702884
V_{cost}- 3	n-expl	800	0.22	0.33	800	0.020	0.026	1350882	1054327

Table 6. Comparison between reactor performance as a function of channel width

Unlike the previous case, where inlet flow rates were kept constant, an increase in channel width keeping the mean gas velocity and the value of t_{rm} constants affects significantly the outlet conversions. In this case the amount of reactants flowing through the reactor per unit catalyst volume and, then, GHSV increases (compare 1st and 5th rows in Table 5).
Increasing channel widths from their reference case value ($W_{c\text{-}sr}$ = 2 mm and $W_{c\text{-}co}$= 1) at constant gas inlet velocity leads to methane conversion reduction because: a) the catalyst amount becomes insufficient for the amount of reactants fed in the reactor and b) the external mass transfer resistances play a stronger role. The overall reaction heat fluxes remain the same as channel width increases, leaving a similar amount of sensible heat to be used for heating up larger amounts of reactants. This results in lower temperatures along the reactor.

4.6 Influence of catalyst thickness

The influence of catalyst thickness, δ_c, on the reactor behaviour was studied by keeping constant the reactants mass flow rates. The reactor operation was simulated for three values of catalyst thickness, i.e. 200, 100, and 50 μm while keeping all the other parameters at their reference case values but for what concerns the inlet methane concentration in the combustion channel that was at non explosive level. This with respect to the reference case corresponds to decreasing GHSV of factors 2 and 4, respectively. Changes in the catalyst thickness influence considerably both thermal behaviour and outlet conversions.
As above the comparison is made through the methane conversions achieved in the two cases both in the steam reforming and in the combustion channels. The results are reported in Table 7. It is evident that the loss of performance due to a decrease of 50% of δ_c from 200 to 100 μm is almost negligible. This is mainly due to the conservative parameters used for defining the catalyst layer characteristics (i.e. mean pore radius and tortuosity) that results in a very impervious path for diffusing gases. However, when δ_c is further decreased, methane conversion both in the combustion and in the reforming section significantly decrease. The hydrogen yield does not change too much within the limits of the three cases analyzed.

δ_c, μm		T_{in}, K	$X_{ch4\text{-}co}$	$X_{ch4\text{-}sr}$	T_{max}, K	$t_{rm\text{-}co}$, ms	$t_{rm\text{-}sr}$, ms	$GHSV_{co}$, h^{-1}	$GHSV_{sr}$, h^{-1}	φ_{H2}
200	n-expl	800	0.36	0.45	827	0.020	0.026	900588	702884	3.44
100	n-expl	800	0.35	0.45	827	0.020	0.026	1801176	1405768	3.44
50	n-expl	800	0.27	0.38	800	0.020	0.026	3602352	2811536	3.42

Table 7. Comparison between reactor performance as a function of catalyst thickness

5. Discussion

As seen in the previous section (4), there are several operating parameters that influence the performances of the system. They are typical of reacting systems and can be summarized as GHSV's, t_{mr}'s and inlet gas temperatures. The particularity of the present case is the simultaneous occurrence of two coupled reactions, one exothermic and the other endothermic, in which the extent of the second depends on the extent (heat produced) of the first and the effectiveness of the heat transferred. In addition, the coupling of the two reactions does not exclude to have for each set of values of the mentioned parameters pertaining to one reaction several sets of parameters for the other reaction. This makes the system quite complex and difficult to analyze. However, some general considerations can be drawn.

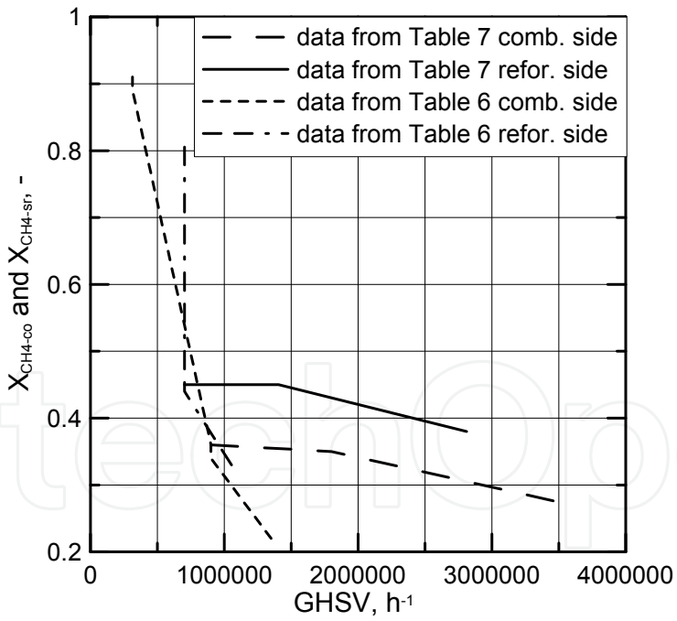

Figure 11. Methane conversions in the combustion and reforming sides of the reactor as a function of GHSV for various operating conditions available in Table 6 and 7

The first is that, as expected, GHVS plays a key role in determining the reactor performances although this is supported by only a part of the data. For instance data in Table 7, pertaining to simulations of the influence of such a parameter, carried out by changing GHSV in the same way for both sections of the reacting system, shows a clear effect of GHSV: the reactor

performance decreases as GHSV increases on both sides of the reactor. Such an influence does not appear strong, the conversion change being about 20% against GHSV variations of a factor 4 (Figure 11). The influence of GHSV is more evident from data in Table 6, pertaining to simulations of the influence of t_{mr}. In fact, also in this case a clear trend appears and the influence, even though in the same direction of the previous case, appears much stronger since with respect to a GHSV change of about 20%, the methane conversion varies by a factor 4 (Figure 11). Such a strong influence is due to the combined effect of t_{mr} especially on the combustion side of the reactor (cfr. Table 6). Instead, for data in Table 5 pertaining to simulations of the reliability of 2D and 3D models and the effect of gas inlet temperature, it is not possible to highlight a clear influence.

The comparison between the results obtained with the 2D and 3D models under the same operating conditions have evidenced differences in the performance of the reactor not large but significant. When we move from 2D to 3D models, such differences result in an increase from 5 to 20% of both $X_{ch4\text{-}co}$ and $X_{ch4\text{-}sr}$, which reflects a different thermal behavior of the reacting system and influence also the hydrogen yield. It is worth noting that the computation time required in the two cases is very different. Specifically, using an HP xw8400workstation equipped with 2 Xeon processors and 4 GB of RAM a 2D simulation takes on the average about 20 minutes with respect to 50-60 hours necessary in the 3D case.

It is impossible by now to establish which is the more correct or the more reliable. In particular, it should be assessed if 2D simulations are suitable for purpose of reactor design and experimental data interpretation. The answer should come from the comparison of the results of such simulations with experimental data obtained with a real reactor geometrically comparable, operated under conditions as much as similar to those fixed for the simulations. This represents argument for coming work of the authors.

Further interesting aspects to be studied are the simulation of unsteady-state conditions and, specifically, of the system start-up and of the system response to small changes in the gas feeding flow rates and temperatures.

6. Conclusions

Methane steam reforming coupled with methane catalytic combustion by means of indirect heat transfer in a surface-bed catalytic reactor was studied by 2D and 3D models. The reactor consists of a central reforming channel and two lateral combustion channels. A reference case for what concerns operating conditions and reactor geometry was chosen and its simulation was carried out. Changes of reactor performance as consequence of operating parameters and reactor geometry variations were analyzed with respect to the reference case.

The simulation showed that suitable amount of fuel and adequate catalyst activity in the combustion channel can provide enough heat to simultaneously heat up the reaction mixture and drive the endothermic process. The proximity between the heat source and the heat sink increases the efficiency of heat transfer resulting in transverse temperature gradients do not exceeding, generally, 0.7 K across the metallic wall and 20 K across the gas in the channel. Decrease of transverse temperature differences and intraphase mass transfer resistances have the global effect of reducing the reactor dimension and the catalyst amount.

The influence of channels width, and catalyst layer thickness on reactor behaviour was also studied. At constant inlet flow rates, changes of channel width in the range 1–2 mm do not introduce significant differences in the reactor performance. Rather small differences in the

catalyst axial temperature profiles and outlet methane conversions are observed. In contrast, altering the channel width at constant inlet velocities has strong influence. Larger channel width results in lower conversion and smoother axial temperature profiles. Intraphase resistances are present even for catalyst thickness of micrometers for both reforming and combustion processes. Increasing GHSV, that is the inlet flow rate/catalyst volume ratio, leads to lower outlet conversions. Due to different effect of catalyst layer thickness on reforming and combustion channels, there are significant changes in the reactor temperature profile. Results indicate that steam reforming of methane in a surface-bed reactor is feasible provided that mass flow rates, channels width, catalyst loadings and thickness are properly designed.

7. Notation

c_p	specific heat, J/(mol K)
c	concentration, mol/m^3
D_{eff}	effective diffusion coefficient, m^2/s
D	molecular diffusion coefficient, m^2/s
GHSV	gas hourly space velocity, h^{-1}
k	thermal conductivity, W/(m K) or reaction rate constant
K_e	equilibrium constant
M	molecular weight, kg/mol
LEL	lower explosivity limit, vol %
$\vec{n}$	unit vector perpendicular to the flux surface
N	molar flux at the boundary, mol/(m^2 s)
p	partial pressure, bar
P	total pressure, bar
q	thermal flux at the boundary, J/(m^2 s)
r	reaction rate, various dimensions (see eq.s 1', 2' and 3')
R_p	catalyst pore radius, nm
STP	standard temperature and pressure (298 K and 101 10^3 Pa)
t	time, s
T	temperature, K
ts	transverse surface
u_x	Velocity component on the x coordinate
$\vec{v}$	velocity vector
v	normal component of velocity at the channel ingress
x	axial coordinate, m
X	conversion
y	transverse coordinate, m
W_c	distance between the reactor plates, m
z	vertical coordinate, m
Greek letters	
ΔH^0_r	heat of reaction at reference state conditions , KJ/mol
δ_c	catalyst thickness, μm
ε	catalyst porosity
φ	atomic diffusion volume or chemical reaction yield

θ	stoichiometric coefficient
ρ	density, kg/m^3
τ	catalyst tortuosity

Subscripts and superscripts

cat	catalyst
co	combustion
CH4	methane
H2	hydrogen
in	inlet
i	chemical species
j	channel
k	reaction
l	phase
rm	mean residence
s	metal sheet
sr	steam reforming
0	channel ingress
1	reforming reaction
2	water gas shift reaction
3	combustion reaction

8. Acknowledgements

The authors gratefully acknowledge the financial support of MIUR under grant PRIN n° 2006094333004.

9. References

Akers, W.W. & Camp, D.P. (1955) Kinetics of the methane–steam reaction. *A.I.Ch.E. Journal*, Vol. 1, 471–475. ISSN:0001-1541.

Allen, D.W., Gerhard, E.R. & Likins Jr., M.R. (1975) Kinetics of the Methane–Steam Reaction. *Ind. Eng. Chem. Proc. Des. Dev.*, Vol. 14, No. 3, 256-259, ISSN:0196-4305.

Aparicio, L., (1997) Transient Isotopic Studies and Microkinetic Modeling of Methane Reforming over Nickel Catalysts. *Journal of Catal.*, Vol. 165, No. 2, 262-274 ISSN: 0021-9517.

Avci, A.K., Trimm, D.L. & İlsen Önsan, Z. (2001) Heterogeneous reactor modeling for simulation of catalytic oxidation and steam reforming of methane. *Chem. Eng. Sci.*, Vol. 56, No 2, 641-649 ISSN:0009-2509

Bridger, G.W. (1980) The steam reforming of hydrocarbons. *Catalysis*, Vol. 3, 39-69, ISSN:0140-0568.

Cao, C., Wang, Y. & Rozmiarek R.T. (2005) Heterogeneous reactor model for steam reforming of methane in a microchannel reactor with microstructured catalysts. *Catal. Today*, Vol. 110, No 1-2, 92–97, ISSN: 0920-5861.

Craciun, R., Shereck, B. & Gorte, R.J. (1998) Kinetic studies of methane steam reforming on ceria-supported Pd. *Catal. Lett.*, Vol. 51, No. 3–4, 149-153, ISSN: 1011-372x.

Crowl, D.A. & Louvar, J.F. (2002) *Chemical Process Safety: fundamentals with applications* 2nd ed., Prentice Hall PTR, Upper Saddle River, NJ, USA. ISBN: 0-13—018176-5

De Deken, J. C., Devos, E. F., & Froment, G. F. (1982). Steam reforming of natural gas. Intrinsic kinetics, diffusional influences and reactor design. ACS Symposium Series, 196, 181–197, ISSN:0097-6156

Ehrfeld, W. & Hessel, V., Lowe, H. (2000) *Microreactor*, Wiley-VCH Verlag GmbH, D-69469, ISBN Weinheim, Germany.

Gosiewski, K. (2001) Simulations of non-stationary reactors for catalytic conversion of methane to synthesis gas. *Chem. Eng. Sci.*, Vol. 56, No 4, 1501-1510 ISSN

Groppi, G., Belloli, A., Tronconi, E., Forzatti, P. (1995). A comparison of lumped and distributed models of monolith catalytic combustors. *Chem. Eng. Sci.*, Vol. 50, No. 17, 2705–2715. ISSN:0009-2509

Holladay, J.D., Wang, Y. & Jones, E. (2004) Review of Developments in Portable Hydrogen Production Using Microreactor Technology. *Chem. Rev.*, Vol. 104, No 10, 4767-4790 ISSN: 0009-2665.

Hou, K. & Hughes, R. (2001) The kinetics of methane steam reforming over a Ni/α-Al_2O_3 catalyst. *Chem. Eng. Journal*, Vol. 82, No. 1-3, 311-328 ISSN: 1385-8947

Jamal, Y. & Wyszynski, M. L. (1994). On-board generation of hydrogen-rich gaseous fuels: a review. *Int. J. of Hydrogen Energy*, Vol. 19, No. 7, 557-572, ISSN: 0360-3199.

Jensen, K.F. (2001) Microreaction engineering : is small better?. *Chem. Eng. Sci.*, Vol. 56, No 2, 293-303. ISSN:0009-2509

Kolios, G., Gritsch, A., Glo1ckler, B. & Sorescu G. (2004) Novel Reactor Concepts for Thermally Efficient Methane Steam Reforming: Modeling and Simulation. *Ind. Eng. Chem. Res.*, Vol. 43, No 16, 4796-4808, ISSN:0888-5885

Kruger, P., Blakeley, J. & Leaver, J. (2003) Potential in New Zealand for use of hydrogen as a transportation fuel. *Int. J. of Hydrogen Energy*, Vol. 28, No. 8, 795–802, ISSN: 0360-3199.

Kvamsdal, H.M., Svendsen, H.F., Hertzberg, T. & Olsvik, O. (1999) Dynamic simulation and optimization of a catalytic steam reformer. *Chem. Eng. Sci.*, Vol. 54, No. 13-14, 2697-2706. ISSN:0009-2509

Lerer, M., Duic, N., Alves, L.M. & Carvalho, M.G. (2006) H_2 RES, energy planning tool for increasing the penetration of renewable energy sources in island energy supply. In: *New and Renewable Technologies for Sustanaible Development.* M.G. Carvalho and N.H. Afgan (Ed .s), 15-30, World Scientific, ISBN: 10 981-270-505-8, Singapore.

Lerou, J.J. & Ng, K.M. (1996) Chemical reaction engineering: A multiscale approach to a multiobjective task. *Chem. Eng. Sci.*, Vol. 51, No 10, 1595-1614 ISSN:0009-2509.

Lincoln, S.F. (2006) *Challenged Earth*, ch.7, Imperial College Press, ISBN: 1-86094-526-0, London

Loffler, D. G., Faz, C. F., Sokolovskii, V. & Iglesia, E. (2002) Catalytic separator plate reactor and method of catalytic reforming of fuel to Hydrogen. PCT Int. Appl., WO 02/28769 A2.

Luna, C. & Becerra, A.M. (1997) Kinetics of methane steam reforming on a Ni on alumina-titania catalyst. *React. Kinet. Catal. Lett.*, Vol. 61, No. 2, 369-374, ISSN: 0133-1736.

Marschner, F., Renner, H.J. & Boll, W. (2005) Electronic Encyclopedia, Release 2005, 7th ed. in: *Ullmann's Encyclopedia of Industrial Chemistry*, M. Bohnet, et al. (Eds.), Vol. a12, John Wiley & Sons, ISBN-13: 978-3-527-30385-4

Moore, R. B. & Raman, V. (1998) Hydrogen infrastructure for fuel cell transportation. *Int. J. of Hydrogen Energy*. Vol. 23, No 7, 617-620, ISSN: 0360-3199..

Perry, R.H. & Green, D.W., (1999) *Perry's Chemical Engineers' Handbook* (7th Ed.), McGraw-Hill. ISBN: 0-07-049841-5

Robbins, F. A., Zhu, H. & Jackson, G.S. (2003) Transient modeling of combined catalytic combustion/CH_4 steam reformng. *Catal. Today*, Vol. 83, No 1-4, 141–156, ISSN: 0920-5861.

Rostrup-Nielsen, J.R., Christiansen, L.J. & BakHansen, J.H. (1988) Activity of steam reforming catalysts: Role and assessment. *Appl. Catal.*, Vol. 43, No 2, 287-303, ISSN:0166-9834.

Rostrup-Nielsen, J.R. (1995) Innovation and the catalytic process industry - the science and challenge. *Chem. Eng. Sci.*, Vol. 50, No 24, 4061-4071, ISSN:0009-2509

Rostrup-Nielsen, J.R., Dybkjaer, I. & Coulthard, G.R.G. (2001) Topical Conf. Proc. AIChE Spring National Meeting, Houston, TX, April, Paper No. 1.

Rostrup-Nielsen, J.R. (2004) Fuels and Energy for the Future: The Role of Catalysis. *Catal. Rev. - Science and Engineering*, Vol. 46, No. 3–4, 247-270, ISSN:0161-4940.

Schubert, K., Brandner, J., Fichtner, M., Linder, G., Schyhulla, U. & Wenka, A. (2001) Microstructure devices for applications in thermal and chemical process engineering. *Microscale Thermophys Eng.*, Vol 5, No 1, 17-39, ISSN:1089-3954.

Tronconi, E. & Groppi, G. (2000) A study on the thermal behavior of structured plate-type catalysts with metallic supports for gas/solid exothermic reactions. *Chem. Eng. Sci.* Vol.: 55, Issue: 24, December, 6021-6036, ISSN:0009-2509

Wang, Y., Johnson, B.R., Cao, C., Chin, Y., Rozmiarek, R.T., Gao, Y., Tonkovich, A.L. (2005) Engineered catalysts for microchannel reactor applications, In: *Microreactor Technology and Process Intensification*, Y. Wang, J. Holladay (Eds.), 65-73, ACS Symposium Series, Vol. 914, ISBN-13: 9780841239234

Xu, J. & Froment, G.F. (1989a) Methane steam reforming II. Diffusional limitations and reactor simulation. *A.I.Ch.E. Journal*, Vol. 35, No. 1, 97-103 ISSN:0001-1541.

Xu, J. & Froment, G.F. (1989b) Methane steam reforming, methanation and water-gas shift. I. Intrinsic kinetics. *A.I.Ch.E. Journal*, Vol. 35, No. 1, 88-96, ISSN:0001-1541.

Zanfir, M. & Gavriilidis, A. (2003) Catalytic Combustion Assisted Methane Steam Reforming. *Chem. Eng. Sci.*, Vol. 58, No 17, 3947– 3960, ISSN:0009-2509

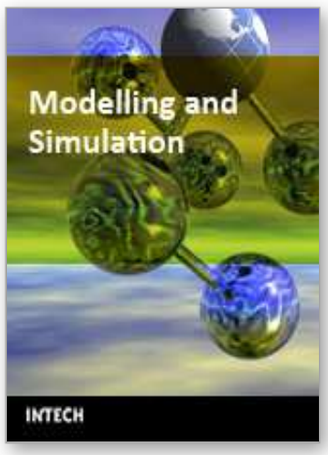

Modelling and Simulation

Edited by Giuseppe Petrone and Giuliano Cammarata

ISBN 978-3-902613-25-7
Hard cover, 688 pages
Publisher I-Tech Education and Publishing
Published online 01, June, 2008
Published in print edition June, 2008

This book collects original and innovative research studies concerning modeling and simulation of physical systems in a very wide range of applications, encompassing micro-electro-mechanical systems, measurement instrumentations, catalytic reactors, biomechanical applications, biological and chemical sensors, magnetosensitive materials, silicon photonic devices, electronic devices, optical fibers, electro-microfluidic systems, composite materials, fuel cells, indoor air-conditioning systems, active magnetic levitation systems and more. Some of the most recent numerical techniques, as well as some of the software among the most accurate and sophisticated in treating complex systems, are applied in order to exhaustively contribute in knowledge advances.

How to reference

In order to correctly reference this scholarly work, feel free to copy and paste the following:

Salvatore Vaccaro and Paolo Ciambelli (2008). Modeling of Surface-bed Reactor for Endothermic and Exothermic Reactions Coupling, Modelling and Simulation, Giuseppe Petrone and Giuliano Cammarata (Ed.), ISBN: 978-3-902613-25-7, InTech, Available from: http://www.intechopen.com/books/modelling_and_simulation/modeling_of_surface-bed_reactor_for_endothermic_and_exothermic_reactions_coupling

INTECH
open science | open minds

InTech Europe
University Campus STeP Ri
Slavka Krautzeka 83/A
51000 Rijeka, Croatia
Phone: +385 (51) 770 447
Fax: +385 (51) 686 166
www.intechopen.com

InTech China
Unit 405, Office Block, Hotel Equatorial Shanghai
No.65, Yan An Road (West), Shanghai, 200040, China
中国上海市延安西路65号上海国际贵都大饭店办公楼405单元
Phone: +86-21-62489820
Fax: +86-21-62489821

IntechOpen